A&A 390, 281–287 (2002)
DOI: 10.1051/0004-6361:20020705


Astronomy & Astrophysics

# A water maser flare in W49N

## The superposition of the spectra of two component masers

J. J. Zhou[1,2], X. W. Zheng[1], and Y. X. Chen[1]

[1] Department of Astronomy, Nanjing University, Nanjing 210093, PR China
[2] Urumqi Astronomical Station, Chinese Academy of Science, Xinjiang, 830011, PR China

Received 6 August 2001 / Accepted 7 May 2002

**Abstract.** We report the results of our short time scale monitoring observations of W49N. Three water maser features were found to show obvious variations in flux density, line width and center velocity. Over a period of about 22 days, the −88.3, −56.9 and −12.8 km s$^{-1}$ features declined linearly in flux density at rates of 57, 113, 98.8 Jy per day, respectively. The line widths of the −56.9 and −12.8 km s$^{-1}$ features increased at rates of ∼0.022 and ∼0.046 km s$^{-1}$ per day, respectively, while the line width of the −88.3 km s$^{-1}$ feature increased at a rate of 0.01 km s$^{-1}$ per day during the first 17 days and decreased at a rate of 0.017 km s$^{-1}$ per day during the remainder of the days. All three features show a systematic shift of ∼1 km s$^{-1}$ in center velocity. We propose a model based on the superposition of the spectra of two maser clouds to explain the variations of these maser features: two rigidly rotating, unsaturated spherical maser clouds during the declining phase reach the same line-of-sight velocity, then they depart from each other because of their relative acceleration.

**Key words.** masers-stars: formation-ISM: individual objects: W49N

## 1. Introduction

W49N is one of the strongest water maser sources in the Galaxy. Observations suggest that the individual water masers are clustered in a region with a size of $\sim 3 \times 10^{17}$ cm (Gammon 1976). The maser features seem to be grouped into several active centers. All these active regions are excited by one star or a cluster of stars, they usually contain low-velocity maser features, some of them also contain high-velocity ones (Litvak 1971; Gammon 1976; Liljeström et al. 1989). The proper motion measurements of water maser features indicate that these maser clusters are expanding from a common center (Gwinn et al. 1988). Within a given center of activity, the higher-velocity features are more spatially dispersed and show more pronounced time variabilities than the lower-velocity features (White 1979; Batchelor et al. 1980; Gwinn 1994a,b). The individual maser features have diameters $\leq 10^{13}$ cm (Batchelor et al. 1980; Gwinn 1994a,b). All of the water masers are produced in the circumstellar material where strong stellar wind interacts with the ambient material (MacLow & Elitzur 1992; Gwinn 1994a,b). The variability of water masers in W49N has been studied since its discovery (Litvak 1971; Sullivan 1973; Gammon 1976). The water masers in W49N show short and long time scale variations. The short-time scale monitoring observations indicate that water maser features in W49N often show dramatic variations in flux density, line width and line center velocity. The comprehensive maser outburst statistics of W49N (Liljeström & Gwinn 2000) give typical time scales for maser variability of 53 days for high-velocity maser features and 114 days for low-velocity maser features. The long-time-scale monitoring observations indicate that the variations of the water maser features seem to have a period of 13–14 years. This was ascribed to the variation of the central star or stars in the outflow activity (Liljeström 1993).

Many models have been proposed to explain the variations of the water masers in W49N, including the "light-house" effect (Gammon 1976), the propagation of the shock wave (Gammon 1976; Elitzur et al. 1989), interstellar scintillation (Simonetti et al. 1993), etc. Most of these models are based on the assumption that the maser features observed are single maser spots. However, this may not be true. For example, the VLBI observations of Gwinn (1994a,b) show that the maser features in W49N usually comprise several maser spots. Boboltz et al. (1998) presented a model based on the interacting of the two maser clouds that explains their observation well. Here we propose a similar model, however, with the difference that we take into account the superposition of two maser components.

The objective of our observations is to study the short time scale variations (days to weeks) of water masers. We have obtained some interesting results from the observations of VY CMa, W3(OH), W51M carried out at the same time (see Zheng et al. 1998; Xu & Zheng 2000; Zhou & Zheng 2001). Here we present the observation of W49N. Section 2 briefly describes

*Send offprint requests to*: J. J. Zhou,
e-mail: zhoujj@ms.xjb.ac.cn

the observations and data reduction, Sect. 3 presents the observed results and in Sect. 4 we discuss the possible explanations for the variations observed during our observing session. Section 5 gives an introduction to and discussion of our model. We discuss the uncertainties of our model in Sect. 6. A preliminary conclusion is given in Sect. 7.

## 2. Observations

The monitoring observations and data reduction have been described in previous papers (Zheng et al. 1998; Xu & Zheng 2000; Zhou & Zheng 2001). Here we repeat only the most important facts for the present study. The pointing accuracy of the Delingha telescope is better than 20″ and its HPBW is 4.2′ at 22 GHz. The beam contains the whole region of W49N, so pointing errors could not cause the apparent variabilities of the water masers in W49N. A high resolution 1024 channel AOS was employed as a back end, it has a channel spacing of 12 kHz or a resolution of 0.16 km s$^{-1}$ at 22 GHz. The half-power widths of the maser features cover more than seven channels, thus there was no problem of undersampling of spectral lines. We checked the AOS performance daily during our observations. The measurements suggested that the AOS was in good working state (Zheng & Lei 1998). Observations were made in the position-switching mode and a 1200 K noise diode was used as a second calibrator. We estimated that atmospheric attenuation at zenith was about 0.05 in the observing session. The flux density calibration error was about 20%. The telescope sensitivity is 38 Jy/K after correcting for instrumental effects. In order to eliminate any gain dependence effect of the radio telescope such as polarization effects, all observations were carried out at the same sidereal time. We made several observations every day and took the averaged value of them so as to eliminate the instrumental effects. Moreover, we selected a feature without significant variation as a reference feature and constructed a gain table. Then the gain table was applied for all features in W49N.

## 3. Results

Two typical spectra obtained on September 1 and 14, 1993 are displayed in Fig. 1. There is a complex of low-velocity maser features ranging from −25 to +25 km s$^{-1}$, and other separate features spread over the blueshifted velocity regions ($-115 \leq V_{\rm LSR} \leq -25$ km s$^{-1}$). No strong features appear in the redshifted region (20–52 km s$^{-1}$). This distribution is consistent with previous observations (Gammon 1976; Little et al. 1977). The spectra seem to be greatly simplified comparing with previous spectra (Little et al. 1977; Walker et al. 1982; Liljeström et al. 1989). We found that three maser features (−88.3 and −56.9 and −12.8 km s$^{-1}$, labelled A, B, C respectively in the bottom panel of Fig. 1) show significant variations in flux density, line width and line center velocity.

Figure 2 shows the variations of the features at −56.9, −12.8 and −88.3 km s$^{-1}$ in flux density, line width and center velocity in the left column (denoted with 1), middle column (denoted with 2) and right column (denoted with 3) respectively. The line-narrowing relations of these features are

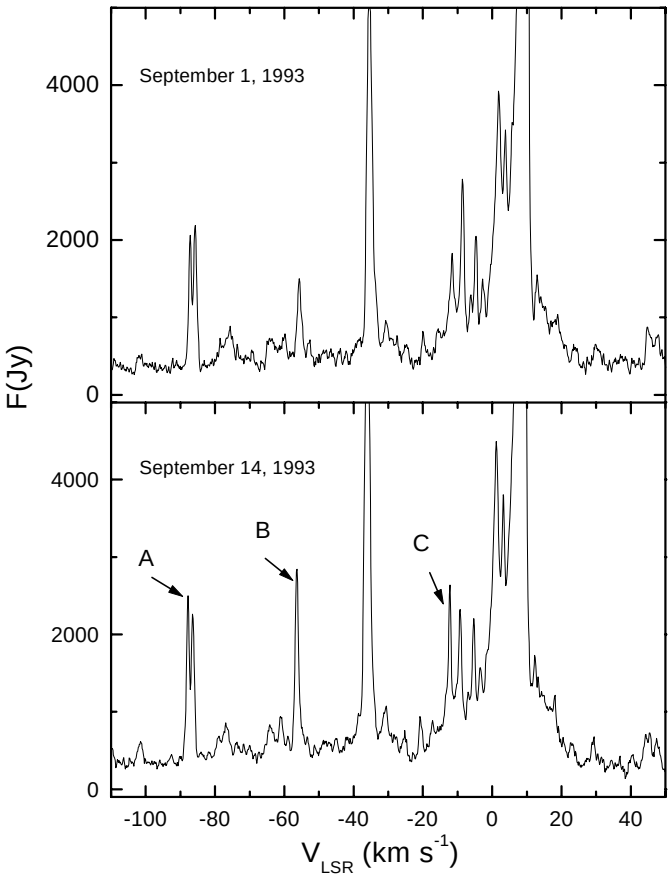


**Fig. 1.** Two typical spectra of water masers on September 1 and 14 of 1993, respectively. Our observations indicate that the −88.3, −56.9 and −12.8 km s$^{-1}$ features labelled A, B and C in the bottom panel show dramatic variations.

shown in panels d of the correspond columns respectively. The line width of the feature at −56.9 km s$^{-1}$ increases successively from 1.18 to 1.66 km s$^{-1}$ at a rate of 0.022 km s$^{-1}$ per day (see panel 1a); during the same period the flux density declines linearly from 4562 Jy to 2069 Jy at a rate of 113 Jy per day (see panel 1b). It is obvious that flux density and line width are anticorrelated. This feature also shows a shift of ∼1 km s$^{-1}$ in center velocity apart from the jump caused by instrumental effects in the first several days (see panel 1c). We find that the other two features show nearly the same variations in center velocity by comparing panel 1c with panel 2c and panel 3c. In panel 1d the relation between the flux density, $F$, and the line width, $\Delta\upsilon$, is plotted on a log-log scale. The data were fitted with a straight line with a slope of −0.3. Similar to the feature at −56.9 km s$^{-1}$, the line width of the feature at −12.8 km s$^{-1}$ increases gradually from 1.33 to 2.34 km s$^{-1}$ at a rate of 0.046 km s$^{-1}$ per day (see panel 2a). The flux density of this feature declines linearly from 3837 Jy to 1664 Jy at a rate of 98.8 Jy per day (see panel 2b). The slope of $\frac{\ln(\Delta\upsilon)}{\ln(F)}$ of the feature is −0.63 (see panel 2d). In contrast with the −56.9 and −12.8 km s$^{-1}$ features, the line width of the feature at −88.3 km s$^{-1}$ increases at a rate of 0.01 km s$^{-1}$ per day in the first 17 days and declines at 0.017 km s$^{-1}$ during the remaining days (see panel 3a). The flux density of the feature, however, declines linearly from 3613 Jy to 2360 Jy

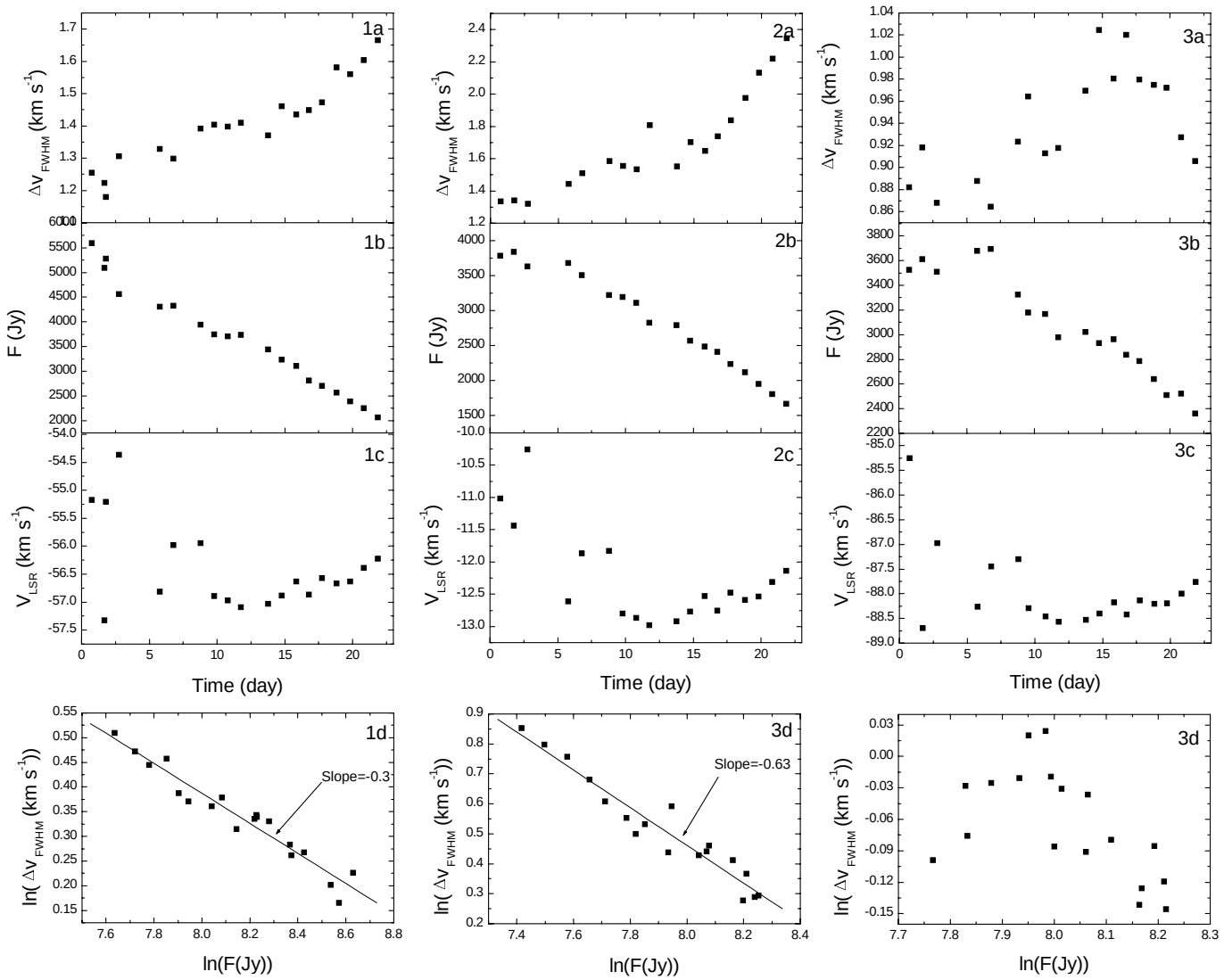


**Fig. 2.** The variations of the features at −56.9, −12.8 and −88.3 km s$^{-1}$ are shown in the left column (denoted with 1), middle column (denoted with 2) and right column (denoted with 3) respectively. During our observing session, the line widths of the feature at −56.9 km s$^{-1}$ increased from 1.18 to 1.66 km s$^{-1}$ (panel 1a), its flux density declined linearly from 4562 Jy to 2069 Jy (panel 1b); the line width of the feature at −12.8 km s$^{-1}$ increased from 1.33 to 2.34 km s$^{-1}$ (panel 2a); its flux density declined linearly from 3837 Jy to 1664 Jy (panel 2b); the line width of the feature at −88.3 km s$^{-1}$ increased in the first 17 days and decreased in the remaining days (panel 3a), its flux density declined linearly from 3613 Jy to 2359 Jy (panel 3b). All three features showed a systematic shift of ∼1 km s$^{-1}$ in the center velocity except for the jumps caused by instrumental effects (panels 1c, 2c and 3c). The −56.9 and −12.8 km s$^{-1}$ features show line-narrowing relations of $\ln(\Delta\nu) \propto -0.3\ln(F)$ and $\ln(\Delta\nu) \propto -0.63\ln(F)$ respectively (panel 1d and 2d). while the feature at −88.3 km s$^{-1}$ shows no such linear relation (panel 3d).

(see panel 3b), the relation between $\ln(\Delta\upsilon)$ and $\ln(F)$ of the feature is shown in panel 3d, which shows no linear relation. We checked the AOS performance daily during our experiment (Zhou & Zheng 2001) and found that the instrumental effects were not responsible for the apparent changes.

## 4. Possible explanation for our observation

The water masers in W49N have a common central energy source; however, only three features showed obvious variations during our observing session, which suggests that the radiation of the central star or stars may have no obvious variation. Some existing models seem to be able to explain our observation.

The line width and flux density of the features at −56.9 and −12.8 km s$^{-1}$ have relations of $\ln(\Delta\nu) \propto -0.3\ln(F)$ and $\ln(\Delta\nu) \propto -0.63\ln(F)$ respectively. These observed line-narrowing relations are not consistent with the relations, $\ln(\Delta\nu) \propto -0.5\ln(F)$, obtained by Mattila et al. (1985) and Liljeström (1993). However, they are similar to those observed by Lada (1981) and Boboltz et al. (1993). Mattila et al. (1985) explained their observation by combining the line width relation of unsaturated masers (Goldreich & Kwan 1974) with the flux relation of saturated masers (which means that two incompatible assumptions were combined). Liljeström (1993) instead explained her observations based on the idea of Strelnitski (1986), that is to say, the line-narrowing relation of saturated

masers might result from changes in the kinematic temperature of the maser cloud. The difference between the observed relations in our experiment and $\ln(\Delta v) \propto -0.5 \ln(F)$ suggests that our observations are not consistent with the above situations.

Deguchi & Watson (1989) proposed that the alignment of a pair of cylindrical masers along the line of sight could explain the enhancement of brightness temperature. Boboltz et al. (1998) presented an interesting model based on the interaction of two maser clouds. In this model, saturated maser radiation produced in a background cloud is amplified by an unsaturated, masing foreground cloud, the rigidly rotating foreground cloud moves across the line of sight in front of a non-rotating background cloud and produces a flaring line accompanied by line-narrowing and a systematic shift in center velocity. Such a model can explain their observation well. However, our calculation indicates that the model is sensitive to the surface rotational velocity and transverse velocity of the foreground cloud. The relative variations in line width of the model are too small compared with those observed in our experiment. Thus the model of Boboltz et al. does not agree with our observations.

The discussions above indicate that existing models cannot explain our observation reasonably. Because the line widths of these three water maser features are very large, they may comprise two or more component maser spots with the same or slightly different line-of-sight velocities (Gwinn 1994a,b). Thus the spectrum of these three water maser features may be the superposition of the spectra of maser spots. We have to construct a model based on the superposition of the spectra of two or more maser spots so as to explain our observation.

## 5. Our model

### 5.1. Description of our model

We think that each of those water maser features showing significant variations during our observing session may comprise two component masers. Similar to the model of Boboltz et al. (1998), we employ two separate maser clouds and background radiation in our model. Here we also assume that these two foreground maser clouds are spherical and unsaturated so that we could calculate their emergent intensity in the same way as Boboltz et al. did. As shown in Fig. 3, two maser clouds 1 and 2 lie in front of the background radiation; both are rotating, unsaturated spherical maser clouds that are in the declining phase. We assume that the acceleration of maser cloud 1 is zero, while maser cloud 2 has a constant, positive acceleration relative to maser cloud 1. They amplify the background radiation and produce the component masers. When these two maser clouds reach the same line-of-sight velocity gradually, the observer will see the flare of the maser. Conversely the observer will see the disappearing of the flare. We simply assume that the background radiation consists of the uniform emission lines of a saturated maser, and that it covers a big enough area to contain maser clouds 1 and 2. We need not know the details of the background source. The motion of maser cloud 2 relative to 1 and the variations of the two maser clouds themselves will determine the flaring line's behavior.

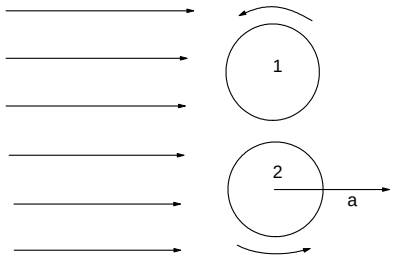


**Fig. 3.** Schematic representation of the two foreground maser clouds and the background radiation. The observer is off to the right. Here we do not specify the details of the background source, it is simply assumed to be a uniform saturated maser emission. Two rigidly rotating spherical maser clouds move along the line of sight. They amplify the background radiation and produce the maser feature we observed. Maser cloud 2 has a acceleration, a, relative to maser cloud 1. The acceleration of maser cloud 1 is assumed to be zero.

To limit the parameters of the model we make a number of simplifying assumptions. The maser clouds 1 and 2 have the same radii and surface rotational velocities, their rotation is a strictly rigid-body rotation, and the axis of the rotation is perpendicular to the line of sight. The internal parameters (density, temperature, composition and opacity) of the two foreground maser clouds are assumed to be uniform and the same. So these two maser clouds have the same thermal and turbulent velocity width, $\Delta v_{\rm D}$. The gains across the maser cloud center, $\tau$, are also the same. it is also assumed that the gaussian distributions of their internal thermal and turbulent motions are the same.

The calculation of the emergent intensity of the two foreground maser clouds is the same as that of Boboltz et al. (1998). We assume that the intensity of the background radiation at frequency $v$ is $I_{v0}$, the source function within the foreground maser cloud is $S_v$, and $S_v \ll I_{v0}$. The intensity of a ray passing through the foreground maser cloud, for a Gaussian distribution of thermal and turbulent motions within the cloud, is $I(v) = I_{v0} \exp(\tau_{\rm c}(1 - \frac{b^2}{r^2})^{0.5} \exp(-[\frac{v-v(b)}{\Delta v_{\rm D}}]^2))$ (Boboltz et al. 1998). Where $\tau_{\rm c}$ is the gain along a path through the center of the cloud, $r$ is the cloud's radius, $\Delta v_{\rm D}$ is the $1/e$ half-width of the distribution of thermal and turbulent motions within the cloud, $v(b)$ is the mean line-of-sight velocity of material along the ray path due to the solid body rotation of the cloud. We compute the total output of the maser cloud at a given velocity by summing the contributing intensities for all uniformly spaced rays that intersect the foreground cloud. After repeating the calculations for all relevant velocities, we get a model spectrum for the foreground maser cloud. Here the intensities are computed only for rays lying in the plane defined by the centers of the two maser clouds and the observer; this simplification does not seriously affect the basic results for a spherical foreground cloud (Boboltz et al. 1998). Therefore, when the difference of the line-of-sight velocity between the two maser clouds is not large enough to resolve their spectra completely, the observer sees the superposition of the spectra of the two foreground maser clouds. The amplitude of the spectrum of any maser cloud declines with the decreasing of the thermal and turbulent velocity width, $\Delta v_{\rm D}$.

When maser cloud 2 moves along the line of sight with a constant positive acceleration relative to maser cloud 1, the velocity difference between maser clouds 1 and 2 changes every day before and after they reach the same line-of-sight velocity, so we get a different spectrum every day. By fitting a Gaussian to the line appearing in these spectra three line parameters are obtained: the amplitude of the line, the center velocity of the line and the $FWHM$ line width. Hence we get a temporal sequence of these three parameters versus observing time, respectively. We do not specify the parameters of the maser clouds, so the actual flux density is not obtained. For comparison with the observed peak flux density values, both the model's amplitudes and the observed peak flux density values are normalized to unity.

There are six adjustable parameters in our model. The radius perpendicular to the line of sight of the spherical maser clouds, $r$; the acceleration of the maser cloud 2 relative to the maser cloud 1, $a$; the $1/e$ half-width of the emission line of the Gaussian distribution of thermal and turbulent velocities within the maser clouds, $\Delta v_{\rm D}$; the decreasing rate of $\Delta v_{\rm D}$ due to the cooling of the maser clouds or some other mechanism, $\Delta v_{\rm D}'$; the surface rotational velocity of the maser clouds, $v_{\rm r}$; the gain across the center of the foreground maser cloud at the rest frequency, $\tau_{\rm c}$. For direct comparison of the model results with the observed data, time as used in the model is expressed in days.

### 5.2. Model results and discussion

The input parameters for the model computation that fit our observations reasonably well are shown in Table 1. Because we need not know the value of the radius, it is not determined. The results of the model are plotted in Fig. 4. It is evident that the kinematical model is efficient in accounting for all of the flare's properties. The parameters used in our model are reasonable for typical masers in star forming regions. The $1/e$ half width of 0.75 km s$^{-1}$ corresponds to an $FWHM$ of 1.25 km s$^{-1}$ for the saturated maser line emitted by the background source, which is a reasonable value (Elitzur et al. 1989). In fact, 0.75 km s$^{-1}$ is the maximum value of $\Delta v_{\rm D}$ in our model. The surface rotational velocities of the maser clouds are also comparable to the model of Boboltz et al. (1998).

Because our observation covers only one part of the entire variation time scale for these maser features, we don't know how they varied before. If the variations of these maser features are caused by the superposition of the spectra of the two component masers, several processes may have been possible before our observation. For example, the two component masers may have been in the declining phase and have continued to decline during our observing session. Or they may have been in the rising phase before our observation and had reached the maximum at the start of our observing session, then begin to decline. For simplicity, we assume the latter case. This means that we begin our model calculation at the time when maser clouds 1 and 2 reach the same line-of-sight velocity, The line-of-sight velocity of cloud 1 remains constant. As the line-of-sight velocity of cloud 2 increases further due to its acceleration relative to cloud 1, the superposition of the two model spectra lessens, the observer sees a decrease of the flux density, an increase of the line width and a systematic shift of the line center velocity, the weakening of these two component maser clouds themselves will enhance such effects. This is probably consistent with the variations of the feature at −56.9 and −12.8 km s$^{-1}$. However, the situation may be different for the feature at −88.3 km s$^{-1}$, because its line width increases in the first 17 days and decrease during the remaining days of our observing session. Perhaps cloud 2 decelerated after the 17th day due to some mechanism that give it a negative acceleration. When this takes place, the observer will see an increase in the peak flux density and an accompanying decrease in the line width. But the weakening of the two component maser clouds themselves, which is denoted by the decrease of the thermal and turbulent velocity width, $\Delta v_{\rm D}$, will eliminate these effects. The correlated decreasing rates are shown in Table 1. If we don't consider the weakening of the component maser clouds in our model, we may not expect to see the flux density decline by more than 50%. The two component maser will separate completely and show up individually in the spectrum.

Our model is a flexible one. As one varies the input parameters slightly, the changes in the computational results are not difficult to understand. The surface rotational velocity of the maser clouds and the relative acceleration between them determines the time scale of the flare. A larger acceleration implies a compressed time scale, while a larger surface rotational velocity means an extended one; it also increases the amplitude of the shift of the center velocity and the line width. Increasing the gain across the center of the foreground maser cloud, $\tau_{\rm c}$, results in a more dramatic variation of the component maser in flux density (Boboltz et al. 1998); this will increases the amplitude of the flare. As we have pointed out, the thermal and turbulent velocity width of the maser cloud is efficient in changing the amplitude of its spectrum and line width, thus the superposition of the spectra of the two component masers will change with the variations of $\Delta v_{\rm D}$. When $\Delta v_{\rm D}$ increases, the observer sees the rise of the peak flux density accompanied with the increase of the line width. When $\Delta v_{\rm D}$ decreases, the observer sees the decrease of the peak flux density accompanied with a decreasing of the line width. If $\tau_{\rm c}$ is fixed, the change of the radius of the component maser has no obvious effect on the superposition of the spectra of the component masers.

The model kinematically generates a systematic shift of 0.383, 0.63 and 0.25 km s$^{-1}$ in center velocity for the features at −56.9, −12.8 and −88.3 km s$^{-1}$, respectively. This supports the idea of Boboltz et al. (1998) that systematic line shifts of less than about 1 km s$^{-1}$ can have a kinematic origin. But these values are smaller than the center velocity shift we observed for the present maser features.

## 6. Uncertainties

Although the calculation and discussion in the last section indicate that our model can explain our observation well, it should be noted that this is based on a series of simplified assumptions. Whether these assumptions are consistent with reality or not may be critical for our results.

**Table 1.** Here $\tau_c$ is the gain through the maser cloud center; $r$ is the radius of the maser clouds; $v_r$ is the surface rotational velocity of the maser cloud; $a$ is the acceleration of maser cloud 2 relative to maser cloud 1; the thermal and turbulent velocity width $\Delta v_D$ is the $1/e$ half-width of the distribution of thermal and turbulent motions within the cloud; $\Delta v_D'$ is the rate of decrease of $\Delta v_D$. For the feature at $-88.3$ km s$^{-1}$, the acceleration of maser cloud 2 relative to maser cloud 1 is 0.03 km s$^{-1}$ per day in the first 17 days and $-0.03$ km s$^{-1}$ per day during the remaining days of our observation.

| parameters | the feature at $-56.9$ km s$^{-1}$ | the feature at $-12.8$ km s$^{-1}$ | the feature at $-88.3$ km s$^{-1}$ |
|---|---|---|---|
| $\tau_c$ | 2.5 | 2.5 | 2.5 |
| $r$ | 3 | 3 | 3 |
| $v_r$ | 0.96 km s$^{-1}$ | 0.8 km s$^{-1}$ | 0.5 km s$^{-1}$ |
| $a$ | 0.06 km s$^{-1}$ per day | 0.045 km s$^{-1}$ per day | 0.03 km s$^{-1}$ per day ($t \leq 17$ days) |
| | | | $-0.01$ km s$^{-1}$ per day ($t \geq 17$ days) |
| $\Delta v_D$ | 0.75 km s$^{-1}$ | 0.75 km s$^{-1}$ | 0.58 km s$^{-1}$ |
| $\Delta v_D'$ | 0.0012 km s$^{-1}$ per day | 0.0016 km s$^{-1}$ per day | 0.002 km s$^{-1}$ per day |

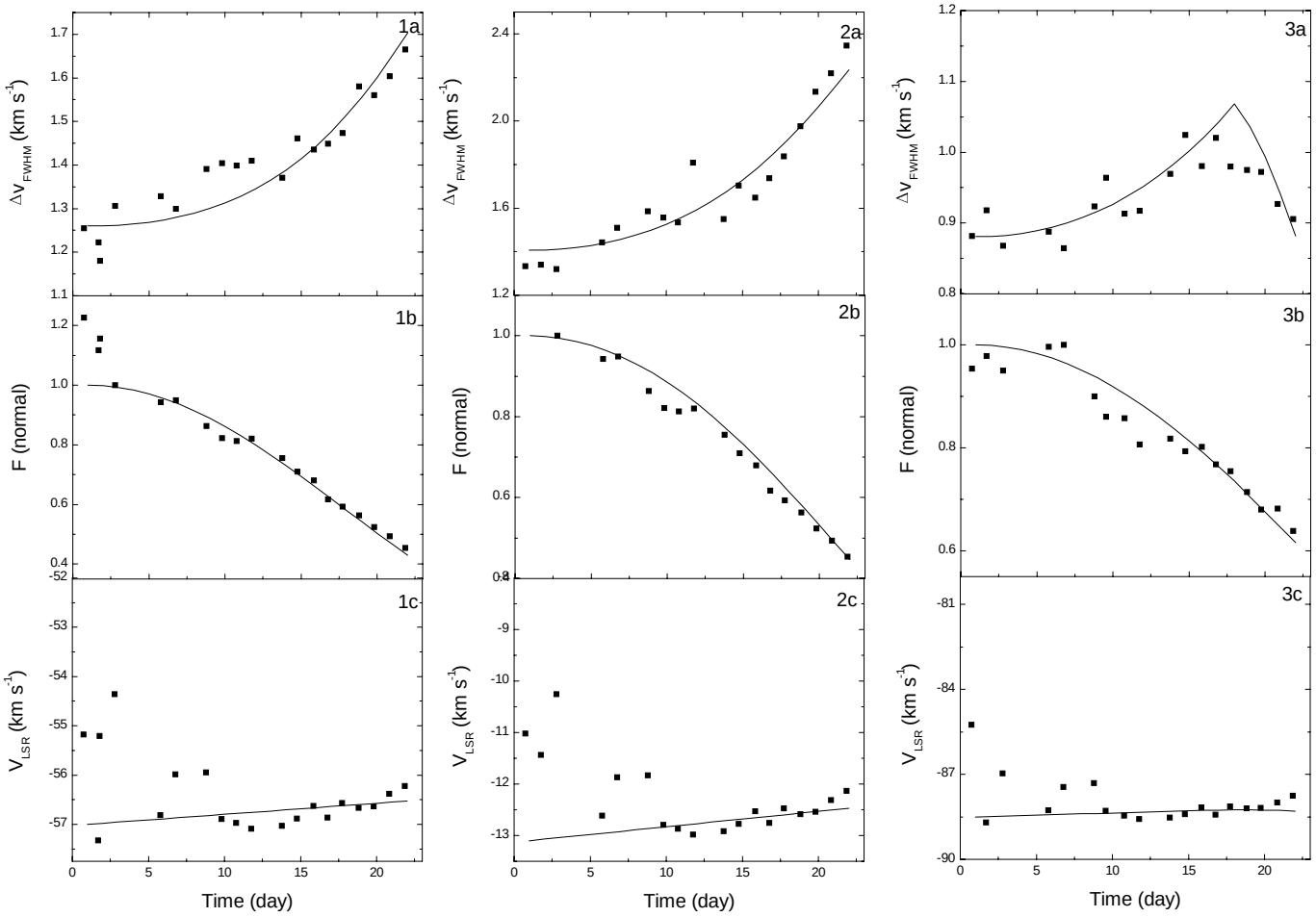


**Fig. 4.** The observed flux density (solid dots) and the model results (solid line) for the line width (a), flux density (b) and line center velocity (c) of the feature at $-56.9$ km s$^{-1}$ (left column), the feature at $-12.8$ km s$^{-1}$ (middle column) and the feature at $-88.3$ km s$^{-1}$ (right column).

It should be noted that the component masers in our model are maser spots rather than the maser features appearing in the single dish spectrum. VLBI observations (Gwinn 1994a,b) show that the water maser features in W49N usually consist of several maser spots clustered in position and velocity; the size of the maser spots is about 1 AU. Thus our assumption that each maser feature comprises two component masers is consistent with reality, though there may actually be more components. Though the neighboring maser features move at velocities larger than 10 km s$^{-1}$ with respect to each other, the maser feature has median internal variations of velocity of $\leq$0.5 km s$^{-1}$ (Gwinn 1994a,b), which represents both the line

width of emission from a single point and subsonic bulk motions. It seems that the turbulent motions of the maser spots within the maser features are completely different from those of the maser features, the maser spots are not affected by turbulent environment. All maser spots within the maser feature may have small accelerations because of their subsonic bulk motions. The assumption that the acceleration of cloud 1 is zero seems to be a problem. If cloud 1 in our model also has a positive acceleration, the center velocity shift of the maser feature will increase. Here we follow the assumption of a spherical unsaturated maser cloud of Boboltz et al. (1998) so as to calculate the emergent intensity in the same way they did. However, the observations indicate that the individual maser features often have very large aspect ratios (Liljeström & Gwinn 2000). It seems that our assumption is inconsistent with the observations, but the spherical maser clouds may show similar observed properties as filamentary maser clouds do because of its beaming effect (Moran 1990). The calculations indicate that the variations of these three water maser features are not consistent with those of unsaturated maser features, this need not indicate that component maser spots are saturated. We also noted that if the assumption that the source function of the maser spots is much less than the intensity of the background radiation no longer holds, our model may fail to explain the observation. The assumption that the two maser clouds have the same size, surface rotational velocities and internal parameters may also be wrong. There are still some uncertainties in our model, but it can be seen that the superposition of the spectrum of component masers may be a reasonable mechanism to explain the variations of the maser features.

## 7. Conclusion

In this paper we present the results of our monitoring observation to W49N. Three features at $-56.9$, $-12.8$ and $-88.3$ km s$^{-1}$ show interesting variations during our observing session. The features at $-56.9$ and $-12.8$ km s$^{-1}$ show line-narrowing relations of $\ln(\Delta v) \propto -0.3 \ln(F)$ and $\ln(\Delta v) \propto -0.63 \ln(F)$ respectively. We propose a model based on the superposition of the spectra of two component masers. We were able to achieve reasonable fits to the normalized flux density data, line width and center velocity with models involving different parameters. It should be noted that our model calculation is based on a series of simplified assumptions, but the reality could be complex. Thus this model may not be a best fit, but it provides us with a new way to consider the variations of the maser features.

## References


Batchelor, R. A., Casewell, J. L., Goss, W. M., et al. 1980, Aust. J. Phys., 33, 139

Boboltz, D. A., Simonetti, J. H., Diamond, P. J., et al. 1993, Astrophysical Masers, ed. A. W. Clegg, & G. E. Nedoluha (Springer Verlag, Heidelberg), 275

Boboltz, D. A., Simonetti, J. H., Dennison, B., et al. 1998, ApJ, 509, 256

Deguchi, S., & Watson, W. D. 1989, ApJ, 340, L17

Elitzur, M., Hollenbach, D. J., & McKee, C. E. 1989, ApJ, 346, 983

Gammon, R. H. 1976, A&A, 50, 71

Goldreich, P., & Kwan, J. 1974, ApJ, 190, 27

Gwinn, C. R., Moran, J. M., Reid, M. J., & Schnep, M. H. 1988, ApJ, 330, 817

Gwinn, C. R. 1994a, ApJ, 429, 241

Gwinn, C. R. 1994b, ApJ, 429, 253

Liljeström, T., Mattila, K., & Anttila, R. 1989, A&AS, 79, 19

Liljeström, T. 1993, Astrophysical Masers, ed. A. W. Clegg, & G. E. Nedoluha (Springer Verlag, Heidelberg), 291

Liljeström, T., & Gwinn, C. R. 2000, ApJ, 534, 781

Litvak, M. 1971, ApJ, 170, 71

Little, L. T., White, G. J., & Riley, P. W. 1977, MNRAS, 180, 639

MacLow, M. M., & Elitzur, M. 1992, ApJ, 393, L33

Mattila, K., Holsti, N., Toriseva, M., et al. 1985, A&A, 145, 192

Moran, J. M. 1990, in Masers in envelopes of young and old stars, Molecular Astrophysics, ed. T. W. Hartquist (Cambridge: Cambridge University Press), 197

Simonetti, J. H., Diamond, P. J., Uphoff, J. A., et al. 1993, Astrophysical Masers, ed. A. W. Clegg, & G. E. Nedoluha (Springer Verlag, Heidelberg), 311

Sullivan, W. T. 1973, ApJS, 25, 393

White, C. J. 1979, MNRAS, 186, 377

Walker, R. C., Matsakis, D. N., & Garcia-Barreto, J. A. 1982, ApJ, 255, 128

Xu, Y., & Zheng, X. W. 2000, A&A, 364, 232

Zheng, X. W., & Lei, C. M. 1998, Chin. Astro. Astrophys., 22, 244

Zheng, X. W., Scalise, J. E., & Han, F. 1998, ApJ, 507, 384

Zhou, J. J., & Zheng, X. W. 2001, Ap&SS, 275, 431